Check for updates

View Article Online
View Journal

ChemComm
Chemical Communications

Accepted Manuscript

This article can be cited before page numbers have been issued, to do this please use: Q. Liu, P. Wei, X. Chen, P. Diao, W. Tian, F. Cui, Y. Han, H. Zhou and S. Kawi, *Chem. Commun.*, 2026, DOI: 10.1039/D6CC01930G.

Volume 54
Number 1
4 January 2018
Pages 1-112

ChemComm
Chemical Communications
rsc.li/chemcomm

ISSN 1359-7345

ROYAL SOCIETY OF CHEMISTRY

COMMUNICATION
S. J. Connon, M. O. Senge *et al.*
Conformational control of nonplanar free base porphyrins: towards bifunctional catalysts of tunable basicity

This is an Accepted Manuscript, which has been through the Royal Society of Chemistry peer review process and has been accepted for publication.

Accepted Manuscripts are published online shortly after acceptance, before technical editing, formatting and proof reading. Using this free service, authors can make their results available to the community, in citable form, before we publish the edited article. We will replace this Accepted Manuscript with the edited and formatted Advance Article as soon as it is available.

You can find more information about Accepted Manuscripts in the Information for Authors.

Please note that technical editing may introduce minor changes to the text and/or graphics, which may alter content. The journal's standard Terms & Conditions and the Ethical guidelines still apply. In no event shall the Royal Society of Chemistry be held responsible for any errors or omissions in this Accepted Manuscript or any consequences arising from the use of any information it contains.

ROYAL SOCIETY OF CHEMISTRY

rsc.li/chemcomm

ChemComm

View Article Online
DOI: 10.1039/D6CC01930G

COMMUNICATION

Double-shelled hollow iron-encapsulated zeolite for enhanced mass transfer and reusability in persulfate activation†

Received 00th January 20xx,
Accepted 00th January 20xx

DOI: 10.1039/x0xx00000x

Qibo Liu,[ac] Wei Pang,[b] Xiaohan Chen,[c] Pinli Diao,[c] Wen Tian,[ab] Feng Cui,[a] Yide Han,*[a] Huanying Zhou,*[b] and Sibudjing Kawi,*[c]

A double-shelled hollow iron-encapsulated zeolite (Fe_2O_3@H-ZSM-5@H-ZSM-5) catalyst was synthesized via a stepwise etching-recrystallization strategy for persulfate activation. The unique double-shelled hollow architecture enhances mass transfer while ensuring ultra-low iron leaching and excellent structural stability, resulting in outstanding reusability.

Antibiotics and dyes have been frequently detected in environmental waters due to their widespread use in medical, livestock farming and industrial applications.[1,2] Their high chemical stability and poor biodegradability enable persistence and accumulation, posing ecological risks and potential threats to human health.[3,4] Conventional treatment technologies often fail to achieve complete removal, thereby motivating the development of more powerful oxidative remediation approaches.[5,6]

Persulfate-based advanced oxidation processes (PS-AOPs) have emerged as effective routes for degrading persistent organic pollutants, owing to their broad pH tolerance, low catalyst demand, and high redox potential of sulfate radicals ($SO_4^{\bullet -}$).[7] Persulfate activation can be achieved via photochemical,[8] thermal,[9] ultrasonic,[10] electrochemical,[11] and transition-metal-mediated pathways.[12] Among these, Iron-based catalysts are promising for efficient reactive oxygen species (ROS) generation in persulfate activation. However, homogeneous iron activation typically requires acidic conditions and suffers from difficult recovery and secondary sludge generation, limiting practical applications.[13] Accordingly, heterogeneous iron-based catalysts, such as supported catalysts,[14] mixed metal oxide catalysts,[15] and doping-modified catalysts,[16] have been extensively explored. Nevertheless, iron species leaching and their poor reusability remain major challenges.

Zeolites are regarded as promising supports for iron species owing to their excellent hydrothermal stability, well-defined microporous structures, and molecular sieving effects.[17] The confinement effect of zeolitic frameworks can enhance the dispersion of iron species during crystallization and effectively suppress iron leaching under catalytic conditions.[18] However, the intrinsically long and narrow micropore channels impose diffusion limitations on PDS and short-lived ROS, resulting in sluggish degradation kinetics. Several strategies, such as creating hollow or hierarchical zeolite architectures, can shorten diffusion pathways and enhance mass transfer.[19] However, etching-induced shell defects may compromise structural integrity, resulting in increased iron species leaching and poor reusability.

Double-shelled hollow zeolite possesses unique advantages, including shortened diffusion pathways, enhanced mechanical stability, and enlarged surface area, these are beneficial for improving mass transfer and catalytic performance.[20] Recently, multi-/double-shelled hollow zeolites have been applied in several catalytic reactions, including hydrocarbon conversion,[21] methanol aromatization,[22] and hydrodeoxygenation processes.[23] Although templating[21] and defect-etching strategies[23] have been reported for constructing double-shelled hollow zeolite, the controllable construction of multi-shelled hollow zeolites with well-confined active sites remains highly desirable. Moreover, their application remains largely unexplored in the PS-AOPs field, particularly for simultaneously enhancing mass transfer and achieving excellent reusability.

Herein, we report a double-shelled hollow iron-encapsulated zeolite (Fe_2O_3@H-ZSM-5@H-ZSM-5) catalyst synthesized via a stepwise etching-recrystallization strategy for PDS activation. We come to a conclusion that (i) the confinement effect of ZSM-5 promotes the uniform dispersion and stabilization of iron species, (ii) the hollow architecture enhances the mass transfer of PDS and ROS, and (iii) the robust double-shelled structure ensures ultra-low iron species leaching and excellent structural stability, enabling outstanding reusability. More importantly, the proposed stepwise etching–recrystallization strategy provides an alternative approach for constructing multi-shelled hollow catalysts and may inspire the design of other multi-shelled hollow-structured catalytic systems.

---

[a] Department of Chemistry, College of Sciences, Northeastern University, Shenyang, 110819, P. R. China. Email: hanyide@mail.neu.edu.cn
[b] Tianjin Key Laboratory of Risk Assessment and Control Technology for Environment and Food Safety, Military Medical Sciences Academy, Academy of Military Sciences, Tianjin 300050, China. Email: zhouhytj@163.com
[c] Department of Chemical and Biomolecular Engineering, National University of Singapore, 4 Engineering Drive 4, 117585, Singapore. Email: chekawis@nus.edu.sg

† Electronic supplementary information (ESI) available. See DOI:10.1039/x0xx00000x

View Article Online
DOI: 10.1039/D6CC01930G

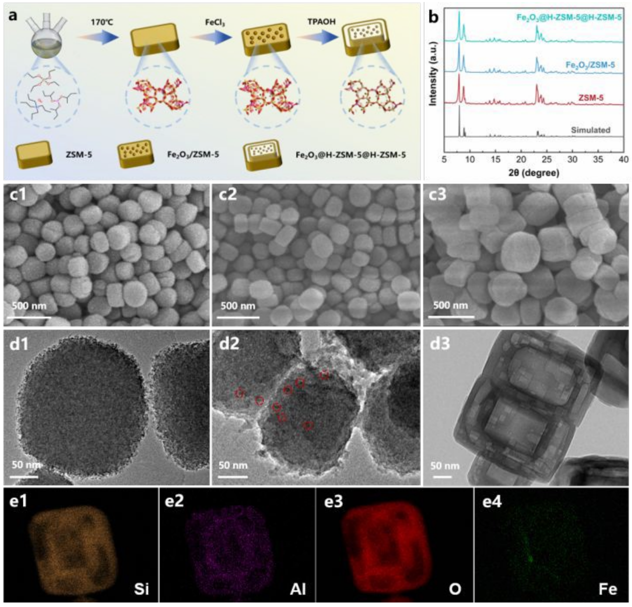

Fig. 1. (a) The schematic illustration of the synthetic route for Fe$_2$O$_3$@H-ZSM-5@H-ZSM-5. (b) XRD patterns of as-prepared samples. SEM images of (c1) ZSM-5, (c2) Fe$_2$O$_3$/ZSM-5, and (c3) Fe$_2$O$_3$@H-ZSM-5@H-ZSM-5. TEM images of (d1) ZSM-5, (d2) Fe$_2$O$_3$/ZSM-5, and (d3) Fe$_2$O$_3$@H-ZSM-5@H-ZSM-5. (e) Elements distribution of Fe$_2$O$_3$@H-ZSM-5@H-ZSM-5.

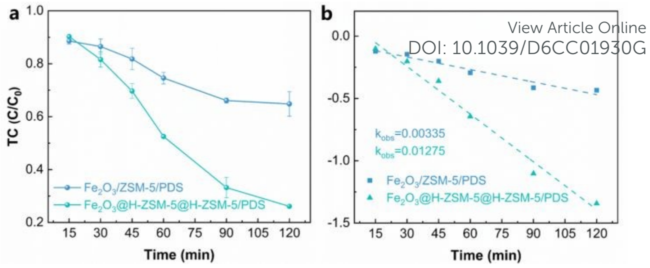

Fig. 2. (a) The TC degradation efficiencies and (b) the values of k$_{obs}$ in different degradation systems.

The schematic illustration of the synthetic route for Fe$_2$O$_3$@H-ZSM-5@H-ZSM-5 is shown in Fig. 1a. The catalyst was constructed via a stepwise etching-recrystallization strategy, which integrates hydrothermal crystallization, controlled etching, and secondary shell growth. First, Fe species were introduced into ZSM-5 via impregnation to form Fe$_2$O$_3$/ZSM-5. Subsequently, controlled alkaline etching was employed to generate the hollow Fe$_2$O$_3$@H-ZSM-5. Then, secondary crystallization was carried out to sequentially grow an S-1 intermediate layer and an outer ZSM-5 shell. Finally, a second alkaline treatment was applied to create the double-shelled hollow Fe$_2$O$_3$@H-ZSM-5@H-ZSM-5 catalyst. Detailed synthetic procedures are provided in the Electronic Supplementary Information (ESI†).

As shown in Fig. 1b, all catalysts exhibit characteristic diffraction peaks corresponding to the MFI structure, indicating the successful formation of the ZSM-5 framework in all samples. Notably, no characteristic diffraction peaks of Fe$_2$O$_3$ are observed in Fe$_2$O$_3$/ZSM-5 and Fe$_2$O$_3$@H-ZSM-5@H-ZSM-5, which may be attributed to the high dispersion or ultra-fine size of Fe$_2$O$_3$ species with crystallite sizes below the detection limit of XRD.[24] The morphology and size of the as-prepared samples were observed by SEM, as shown in Fig. 1c. Both ZSM-5 (c1) and Fe$_2$O$_3$/ZSM-5 (c2) exhibit a typical disc-like morphology with an average diameter of ~250 nm and a thickness of ~160 nm. Moreover, no obvious Fe$_2$O$_3$ aggregates are observed on the surface of Fe$_2$O$_3$/ZSM-5. In contrast, Fe$_2$O$_3$@H-ZSM-5@H-ZSM-5 (c3) displays an ellipsoidal morphology with a larger particle size of ~300 nm, which may be associated with repeated shell growth during the multi-step synthesis processes. As shown in Fig. 1d, both ZSM-5 (d1) and Fe$_2$O$_3$/ZSM-5 (d2) exhibit a totally solid structure. However, Fe$_2$O$_3$ clusters with a size of ~9 nm can be clearly observed in Fe$_2$O$_3$/ZSM-5, suggesting that the ZSM-5 framework effectively confines the growth of Fe$_2$O$_3$ species. Furthermore, SEM and TEM images of Fe$_2$O$_3$@H-ZSM-5 can be found in Fig. S1 (ESI†). Moreover, Fe$_2$O$_3$@H-ZSM-5@H-ZSM-5 displays a well-defined double-shelled hollow structure. The inner cavity has a size of ~180 nm x 110 nm with an inner shell thickness of ~20 nm, while the outer cavity is ~30 nm with an outer shell thickness of ~14 nm, and the overall particle size is ~300 nm x 210 nm, confirming the successful construction of the double-shelled hollow architecture. In addition, no obvious Fe$_2$O$_3$ clusters are observed on the surface of Fe$_2$O$_3$@H-ZSM-5@H-ZSM-5, which may be attributed to the partial migration or loss of iron species during the alkaline etching process, leading to a higher dispersion of the remaining iron species. Furthermore, the elemental mapping (Fig. 1e) shows that Si, Al, O, and Fe are uniformly distributed throughout Fe$_2$O$_3$@H-ZSM-5@H-ZSM-5. The proportion of the main elements in different samples are listed in Table S1 (ESI†). ZSM-5 possesses a Si/Al ratio of 42.95, which is favorable for the formation of the hollow structure. For Fe$_2$O$_3$/ZSM-5, the Si/Al ratio has a slight change, and the iron content is determined to be 4.49 wt%. In contrast, the Si/Al ratio of Fe$_2$O$_3$@H-ZSM-5@H-ZSM-5 increases to 67.51, which is likely related to the repeated shell growth and alkaline etching during the multi-step synthesis processes. Meanwhile, the iron content decreases to 0.90 wt%. Overall, these results confirm the successful construction of Fe$_2$O$_3$@H-ZSM-5@H-ZSM-5 with a double-shelled hollow structure.

Tetracycline (TC) was selected as a representative organic pollutant, and the degradation conditions were optimized as shown in Fig. S2 (ESI †). The optimal degradation conditions were determined as follows: pH 5, 15 mg of Fe$_2$O$_3$@H-ZSM-5@H-ZSM-5, and 30 mg of PDS. As shown in Fig. 2, only 35.2% of TC was removed in Fe$_2$O$_3$/ZSM-5/PDS system within 150 min, with a reaction rate constant (k$_{obs}$) of 0.00335 min^{-1}. This relatively low activity may be attributed to the diffusion limitation of PDS and ROS within the microporous channels of ZSM-5. In contrast, 73.9% of TC was removed in Fe$_2$O$_3$@H-ZSM-5@H-ZSM-5/PDS system, with a k$_{obs}$ value of 0.01275 min^{-1}. Notably, despite the lower iron loading (0.90 wt%), the k$_{obs}$ value is still approximately four times higher than that of Fe$_2$O$_3$/ZSM-5/PDS system. Quantitative calculation further reveals that the utilization efficiency of iron species in Fe$_2$O$_3$@H-ZSM-5@H-ZSM-5 is about 20 times higher than that in Fe$_2$O$_3$/ZSM-5. This significant improvement can be attributed to the hollow structure of Fe$_2$O$_3$@H-ZSM-5@H-ZSM-5, which facilitates the mass transfer of PDS and ROS and shortens the diffusion pathways during the catalytic reaction.

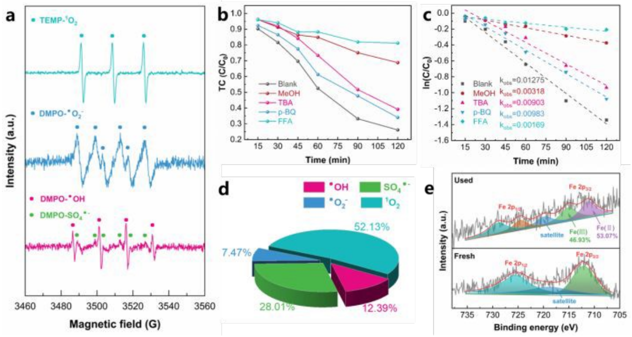

Fig. 3. (a) EPR spectra in Fe_2O_3@H-ZSM-5@H-ZSM-5/PDS system. (b) TC degradation efficiencies and (c) the values of k_{obs} in the presence of various scavengers. (d) Contribution rate of each ROS during the TC degradation process. (e) XPS spectra of Fe 2p of fresh and spent Fe_2O_3@H-ZSM-5@H-ZSM-5.

Electron paramagnetic resonance (EPR) spectroscopy was employed to identify the ROS generated in Fe_2O_3@H-ZSM-5@H-ZSM-5/PDS system. As shown in Fig. 3a, strong signals of DMPO-$^•OH$, DMPO-$^•O_2^-$, and TEMP-$^1O_2$, together with a relatively weak DMPO-$SO_4^{•-}$ signal, can be clearly observed, indicating the involvement of multiple ROS ($^•OH$, $SO_4^{•-}$, $^•O_2^-$, and $^1O_2$) in TC degradation. To further quantify the contribution of each ROS, 100 mM MeOH, 100 mM TBA, 5 mM p-BQ, and 10 mM FFA were added to the reaction system as ROS scavengers.[25] As shown in Fig. 3b and Fig. 3c, the addition of p-BQ only slightly affects the TC degradation efficiency, with a removal rate of 66.00%. In contrast, the addition of FFA significantly suppresses the TC degradation, while the value of k_{obs} decreases from 0.01275 min^{-1} to 0.00169 min^{-1}. The contribution rates of individual ROS were further quantitative calculation, as shown in Fig. 3d. Among these, $SO_4^{•-}$ exhibits a relatively significant contribution rate of 28.01%, highlighting the advantage of PDS as an oxidant. Meanwhile, $^1O_2$ plays a major role, with a contribution rate of 52.13%, which is consistent with the quenching experiment results.[26] Furthermore, as shown in Fig. 3e, iron species in the fresh Fe_2O_3@H-ZSM-5@H-ZSM-5 mainly exist in the form of Fe_2O_3. During the PDS activation process, iron species act as the main active sites, and approximately 53.07% of Fe(Ⅲ) is reduced to Fe(Ⅱ). Based on these results, a possible catalytic mechanism is proposed: PDS is activated by the iron species in Fe_2O_3@H-ZSM-5@H-ZSM-5 to generate multiple ROS, while a portion of Fe(Ⅲ) is reduced to Fe(Ⅱ). Among these ROS, $^1O_2$ plays the predominant role during TC degradation process.

The iron species leaching, structural stability, and reusability of Fe_2O_3@H-ZSM-5@H-ZSM-5 were systematically investigated. The iron species leaching concentration after each reaction was determined using a modified 1,10-phenanthroline method.[27] As shown in Fig. 4a, the iron species leaching concentration after the first cycle is only 0.011 mg L^{-1}, which decreases to below the detection limit after four cycles. Furthermore, the iron species leaching concentration of Fe_2O_3@H-ZSM-5@H-ZSM-5 was compared with previously reported catalysts. As shown in Fig. 4b, the iron species leaching concentration of Fe_2O_3@H-ZSM-5@H-ZSM-5 is significantly lower than that reported in most literatures, and the detailed comparison is shown in Table S2 (ESI†). This result indicates that the double-shelled structure of Fe_2O_3@H-ZSM-5@H-ZSM-5 effectively suppresses the leaching of iron species during the catalytic process due to its double-shell barrier effect. Moreover, the spent catalyst was characterized by XRD (Fig. 4c) and SEM (Fig. S3). The results show that the catalyst still retains the characteristic MFI structure after repeated reactions. Meanwhile, its particle size and morphology show only slight changes, and no obvious structural damage or surface cavities are observed, indicating that Fe_2O_3@H-ZSM-5@H-ZSM-5 possesses excellent structural stability, which is attributed to its robust double-shelled structure. More importantly, the reusability of Fe_2O_3@H-ZSM-5@H-ZSM-5 was tested. As shown in Fig. 4d, after eight consecutive cycles, the TC degradation efficiency decreases by only 8.2% compared with the initial run, demonstrating the outstanding reusability. Overall, the unique double-shelled hollow architecture of Fe_2O_3@H-ZSM-5@H-ZSM-5 not only effectively suppresses the leaching of iron species, but also ensures excellent structural stability, resulting in outstanding reusability during TC degradation process.

View Article Online
DOI: 10.1039/D6CC01930G

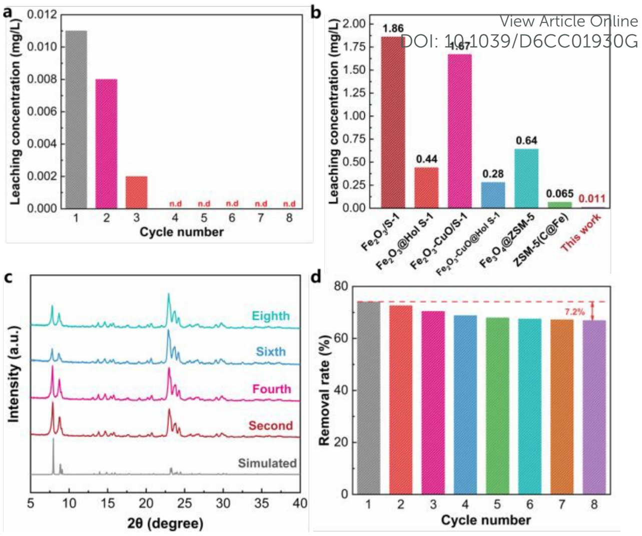

Fig. 4. (a) Iron species leaching concentration after each catalytic cycle. (b) Comparison of iron species leaching concentrations. (c) XRD patterns of the spent Fe_2O_3@H-ZSM-5@H-ZSM-5 catalyst. (d) TC removal rate during repeated catalytic cycles.

To evaluate the practical applicability of Fe_2O_3@H-ZSM-5@H-ZSM-5, a catalyst-loaded membrane was constructed for the degradation of organic pollutants. As illustrated in Fig. 5a, wastewater is pumped into the reactor, where organic pollutants are removed in Fe_2O_3@H-ZSM-5@H-ZSM-5/PDS system, and the treated water is subsequently collected. The water purification setup was further assembled, as shown in Fig. 5b, in which the reactor consists of two sieve plates and a catalyst-loaded membrane. By comparing the fresh and spent membranes, no obvious detachment of Fe_2O_3@H-ZSM-5@H-ZSM-5 is observed on the membrane surface (Fig. 5c-e), indicating that the catalyst-loaded membrane exhibits good structural stability.

To further evaluate the anti-interference capability, the effects of various coexisting anions on TC removal were investigated. As shown in Fig. 5f, the addition of NO_3^-, Cl^-, and HCO_3^- only exhibit minor effects on TC removal at low concentrations, whereas their inhibitory effects becomes more significant with increasing anion concentration. In contrast, the presence of HPO_4^{2-} and SO_4^{2-}

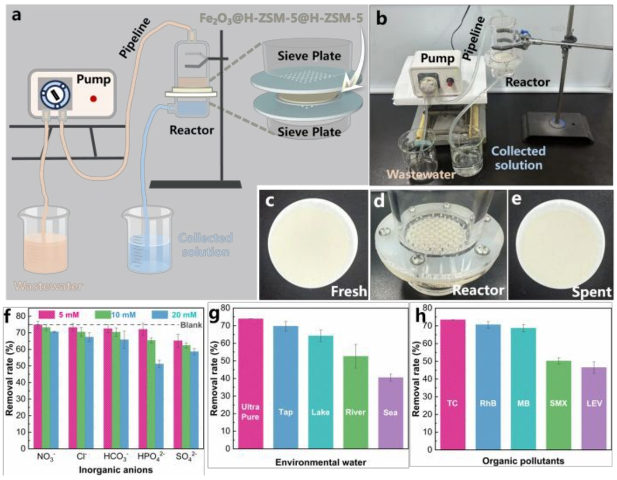

Fig. 5. (a) Schematic illustration and (b) photograph of the membrane reactor for practical organic pollutant removal. (c) The fresh catalyst-loaded membrane, (d) the reactor, and (e) the spent catalyst-loaded membrane. (f) Effects of coexisting anions on TC removal rate. (g) TC removal rate in real environmental water samples. (h) Removal rate of various organic pollutants ([MB] = [RhB] = [LEV] = [SMX] = 10 mg L^{-1}) in the water purification setup.

suppresses the TC removal rate. These phenomena may be attributed to the consumption of ROS by these anions.[28,29] In addition, anions with higher negative charges are more likely to react with ROS, thereby further reducing the TC degradation rate.[30,31] Subsequently, real environmental water samples containing 10 mg L^{-1} TC were introduced into the water purification setup for evaluation. As shown in Fig. 5g, among all tested real water samples, the lowest TC removal rate (40.5%) is observed in seawater. This may be attributed to the more complex composition of seawater, which contains various anions and organic substances that may interfere with the degradation process.[32,33] Finally, the water purification setup was further applied to the removal of other organic pollutants. As shown in Fig. 5h, the removal rates of RhB and MB both exceed 68.7%, indicating the effective purification capability of the water purification setup toward various organic pollutants. Overall, these results demonstrate that the catalyst-loaded membrane-based water purification setup exhibits strong anti-interference capability and promising practical applicability.

In this work, a double-shelled hollow iron-encapsulated zeolite (Fe_2O_3@H-ZSM-5@H-ZSM-5) catalyst was successfully synthesized via a stepwise etching-recrystallization strategy. Benefiting from the hollow architecture, the value of k_{obs} in Fe_2O_3@H-ZSM-5@H-ZSM-5/PDS system is approximately 4 times higher than that in Fe_2O_3/ZSM-5/PDS system. More importantly, owing to its robust double-shelled structure, Fe_2O_3@H-ZSM-5@H-ZSM-5 exhibits an ultra-low iron leaching concentration (0.011 mgL^{-1}) and excellent structural stability, which together endow the catalyst with outstanding reusability, as evidenced by only a slight decrease (8.2%) in TC removal rate after eight consecutive cycles. This stepwise etching-recrystallization strategy provides an alternative approach for constructing multi-shelled hollow catalysts and may inspire the design of other multi-shelled hollow-structured catalysts for AOPs and water purification.

View Article Online
DOI: 10.1039/D6CC01930G

Conflicts of interest

There are no conflicts to declare.

Data availability

Data supporting the findings of this study are available within the article and its Electronic Supplementary Information (ESI†). Additional data are available from the corresponding author upon reasonable request.

Author Contributions

Qibo Liu: Writing – original draft, Methodology, Investigation, Formal analysis, Data curation. Wei Pang: Methodology, Investigation, Formal analysis, Data curation. Xiaohan Chen: Methodology, Investigation, Formal analysis. Pinli Diao: Methodology, Investigation, Funding acquisition. Wen Tian: Methodology, Investigation, Formal analysis, Conceptualization, Data curation. Feng Cui: Writing – original draft, Methodology, Investigation, Formal analysis, Data curation, Validation. Yide Han: Writing – review & editing, Investigation, Funding acquisition, Formal analysis, Conceptualization, Project administration. Huanying Zhou: Investigation, Funding acquisition, Formal analysis, Conceptualization. Sibudjing Kawi: Writing – review & editing, Formal analysis, Conceptualization, Data curation, Funding acquisition, Supervision.

Acknowledgements

This work was supported by the National Natural Science Foundation of China (Grant: 21771032) and the China Scholarship Council (CSC).

References

1 Z. Chen, G. Meng, Z. Han, H. Li, S. Chi, G. Hu and X. Zhao, *J.Colloid Interface Sci.,* 2025, **679,** 67-78.
2 Y. Li, M. Wang, X. Chen, S. Cui, N. Hofstra, C. Kroeze, L. Ma, W. Xu, Q. Zhang, F. Zhang and M. Strokal, *Water Res.,* 2022, **209,** 117906.
3 S. M. Zainab, M. Junaid, N. Xu and R. N. Malik, *Water Res.,* 2020, **187,** 116455.
4 J. Li, D. Wang, S. Zhao, R. Ma, J. Guo, Z. Li, D. Wang, Y. Xuan and L. Wang, *Appl. Catal. B,* 2024, **351,** 124007.
5 A. Raichur and N. Sinha, *Sep. Purif. Technol.,* 2023, **308,** 122830.
6 H. Xiong, S. Dong, J. Zhang, D. Zhou and B. Rittmann, *Water Res.,* 2018, **136,** 75-83.
7 P. Koundle, N. Nirmalkar and G. Boczkaj, *J. Environ. Chem. Eng.,* 2025, **374,** 124107.
8 M. Amasha, A. Baalbaki and A. Ghauch, *Chem. Eng. J.,* 2018, **350,** 132323.
9 Y. Zhou, Y. Xiang, Y. He, Y. Yang, J. Zhang, L. Luo, H. Peng, C. Dai, F. Zhu and L. Tang, *J. Hazard. Mater.,* 2018, **359,** 396–407.
10 R. Yin, W. Guo, H. Wang, J. Du, X. Zhou, Q. Wu, H. Zheng, J. Chang and N. Ren, *Chem. Eng. J.,* 2018, **335,** 145–153.

View Article Online
DOI: 10.1039/D6CC01930G

11 S. Yan, X. Zhang and H. Zhang, *J. Hazard. Mater.,* 2019, **374,** 92–100.
12 X. Zheng, X. Niu, D. Zhang, M. Lv, X. Ye, J. Ma, Z. Lin and M. Fu, *Chem. Eng. J.,* 2022, **429,** 132323.
13 S. Xiao, M. Cheng, H. Zhong, Z. Liu, Y. Liu, X. Yang and Q. Liang, *Chem. Eng. J.,* 2020, **384,** 123265.
14 Y. Zhang, B. Zhang, Y. Teng, J. Zhao and X. Sun, *J. Hazard. Mater.,* 2021, **401,** 123428.
15 L. Fang, K. Liu, F. Li, W. Zeng, Z. Hong, L. Xu, Q. Shi and Y. Ma, *J. Hazard. Mater.,* 2021, **403,** 123669.
16 Z. Jin, Y. Li, H. Dong, S. Xiao, J. Xiao, D. Chu, X. Hou, S. Xiang, Q. Dong and L. Li, *Chem. Eng. J.,* 2022, **448,** 137620.
17 H. Chi, J. Wan, Y. Ma, Y. Wang, M. Huang, X. Li and M. Pu, *J. Hazard. Mater.,* 2020, **398,** 123024.
18 Q. Liu, Y. Wang, X. Sang, J. Bi, N. Liu, X. Zhang, Z. Wang and Y. Han, *Sep. Purif. Technol.,* 2025, **354,** 129369.
19 Q. Liu, J. Bi, Z. Zhai, W. Tian, N. Liu, X. Zhang, Z. Wang, H. Zhou and Y. Han, *J. Environ. Chem. Eng.,* 2025, **13,** 118409.
20 H. Yang, X. Liu, G. Lu and Y. Wang, *Micropor. Mesopor. Mat.,* 2026, **225,** 144-153.
21 J. Xiao, K. Cheng, X. Xie, M. Wang, S. Xing, Y. Liu, T. Hartman, D. Fu, K. Bossers, M. A. Huis, A. Blaaderen, Y. Wang and B. M. Weckhuysen, *Nat. Mater.,* 2022, **21,** 572-579.
22 Q. Ma, T. Fu, Z. Wang, C. Li, X. Wu, N. Yang and Z. Li, *Small,* 2024, **20,** 2308502.
23 G. Chen, P. She, J. Han, J. Li, G. Tian, Y. Sun, Y. Gao, G. Yang, Z. Diao, B. Guan and J. Yu, *Angew. Chem. Int. Ed.,* 2025, **64,** e202424690.
24 S. Andonova, S. Tamm, C. Montreuil, C. Lambert and L. Olsson, *Appl. Catal. B,* 2016, **180**, 775-787.
25 J. Qu, Y. Xu, X. Zhang, M. Sun, Y. Tao, X. Zhang, G. Zhang, C. Ge and Y. Zhang, *Appl. Catal. B,* 2025, **316,** 121639.
26 X. Zou, J. Wang, G. Lv, T. Wang, C. Zhou, Y. Chen, J. Shen, S. Su and Z. Liu, *Micropor. Mesopor. Mat.,* 2023, **360,** 112735.
27 C. Adán, A. Bahamonde, I. Oller, S. Malato and A. Martínez-Arias, *Appl. Catal. B,* 2014, **144,** 269-276.
28 J. Wang, Z. Liao, J. Ifthikar, L. Shi, Z. Chen and Z. Chen, *RSC Adv.,* 2017, **7,** 18696-18706.
29 L. Hu, G. Zhang, M. Liu, Q. Wang and P. Wang, *Chem. Eng. J.,* 2018, **338,** 300-310.
30 Z. Wu, Y. Wang, Z. Xiong, Z. Ao, S. Pu, G. Yao and B. Lai, *Appl. Catal. B,* 2020, **277,** 119136.
31 P. Duan, T. Ma, Y. Yue, Y. Li, X. Zhang, Y. Shang, B. Gao, Q. Zhang, Q. Yue and X. Xu, *Sci. Nano,* 2019, **6,** 1799-1811.
32 L. Niu, G. Zhang, G. Xian, Z. Ren, T. Wei, Q. Li, Y. Zhang, Z. Zou, *Sep. Purif. Technol.,* 2021, **259,** 118156.
33 R. Soltani, M. Mashayekhi, S. Jorfi, A. Khataee, M. Ghanadzadeh and M. Sillanpaa, *Chemosphere,* 2018, **210,** 699-708.

View Article Online
DOI: 10.1039/D6CC01930G

Data availability

Data supporting the findings of this study are included in the article and its ESI.†. Data are also available upon request.